Multispectrum fitting of line parameters for 12C2H2 in the 3.8-μm spectral region

David Jacquemart, Nelly Lacome, Jean-Yves Mandin, Victor Dana, Oleg M. Lyulin, Valery I. Perevalov

Multispectrum fitting of line parameters for $^{12}C_2H_2$ in the 3.8-μm spectral region

D. Jacquemart[1*], N. Lacome[1], J.-Y. Mandin[2], V. Dana[2], O.M. Lyulin [3], V.I. Perevalov [3]

[1] *Université Pierre-et-Marie-Curie-Paris6, Laboratoire de Dynamique, Interactions et Réactivité, CNRS, UMR 7075, Case courrier 49, Bât F 74, 4, place Jussieu, 75252 Paris Cedex 05, France*

[2] *Université Pierre-et-Marie-Curie-Paris6, Laboratoire de Physique Moléculaire pour l'Atmosphère et l'Astrophysique, CNRS, UMR 7092, Case courrier 76, 4, place Jussieu, 75252 Paris Cedex 05, France*

[3] *Laboratory of Theoretical Spectroscopy, Institute of Atmopheric Optics, Siberian Branch, Russian Academy of Sciences, 1, Akademicheskii av.,634055 Tomsk, Russia*

---

[*] Corresponding author. Tel.: + 33-1-44-27-36-82; fax: + 33-1-44-27-30-21.
E-mail address: jacquemart@spmol.jussieu.fr.

Abstract

Using FT spectra (Bruker IFS 120, unapodized FWHM resolution ≈ 0.001 cm^{-1}) of acetylene $^{12}C_2H_2$, absolute positions and intensities have been measured for about 250 lines between 2600 and 2800 cm^{-1} in the $\nu_2 + \nu_5^1$ and $(3\nu_4 + \nu_5)_+^0$ cold bands, and in the $\nu_1 - \nu_5^1$, $\nu_3 - \nu_4^1$, and $\nu_2 + (\nu_4 + \nu_5)_0^+ - \nu_4^1$ hot bands. These measurements improve the accuracy of wavenumbers previously available and lead to individual line intensities for the first time in this spectral region. A multispectrum fitting procedure has been used to retrieve line parameters from 5 experimental spectra recorded at different pressures. The frequencies of the ν_3 band of $^{12}C^{16}O_2$ allowed to perform an absolute wavenumber calibration. The accuracy of the amount of $^{12}C_2H_2$ in the sample has been checked using the $3\nu_5^1$ cold band around 2100 cm^{-1}, and has been estimated to be around $\pm 2\%$. The average absolute accuracy of the line parameters obtained in this work has then been estimated to be ± 0.0002 cm^{-1} for line positions, and $\pm 5\%$ for line intensities. For each studied band, the vibrational transition dipole moment squared value has been determined, as also empirical Herman-Wallis coefficients. A complete line list containing positions and intensities for the 5 strongest bands around 3.8 μm has been set up for atmospheric applications.

Key words: Acetylene; Infrared; Vibro-rotational transitions; Fourier transform spectroscopy; Line intensities; Transition dipole moment; Herman-Wallis factor

1. Introduction

The present paper follows a series of articles devoted to the measurements of intensities of acetylene transitions in the 13.6-μm, 5-μm, and 3-μm spectral regions [1-6]. The 3.8-μm region under study is of interest for atmospheric and astrophysical applications, since it presents strong Q branches that could be detected in atmospheric spectra and used to retrieve concentrations of acetylene. In order to derive the acetylene concentration from atmospheric spectra or from spectra of astrophysical objects, spectroscopic data as line parameters are necessary. As soon as 1961, Wiggins et al. [7] measured line positions in 11 bands located between 2500 and 4150 cm^{-1} with a low resolution of 0.03 cm^{-1}. This set included the 5 bands studied in this work. A decade later, Palmer et al. [8] measured line positions of numerous bands between 1.5 and 15 μm still with a low resolution of 0.04 cm^{-1}. This second set included also the 5 bands studied in this work. It can be noticed that line positions in the $(3\nu_4 + \nu_5)_+^0$ cold band and four hot bands of the 3.8-μm spectral region have also been studied by Plíva [9] and D'Cunha et al. [10] respectively. Values of band intensities around 300 K have been obtained by Koops et al. [11] for the whole 3.8-μm spectral region and by Rinsland et al. [12] for the $\nu_2 + \nu_5^1$ Q branch. No analysis of absolute individual line intensities had been done before the present work. This is probably the reasons why the 3.8-μm region is still missing in the atmospheric and planetary databases as HITRAN [13] and GEISA [14]. The analysis of line positions and intensities in this spectral region will be useful for the global theoretical treatment developed in Refs. [15-18].

About 250 absolute line positions and intensities have been measured between 2600 and 2800 cm^{-1} in the $\nu_2 + \nu_5^1$ and $(3\nu_4 + \nu_5)_+^0$ cold bands, and in the $\nu_1 - \nu_5^1$, $\nu_3 - \nu_4^1$, and $\nu_2 + (\nu_4 + \nu_5)_0^+ - \nu_4^1$ hot bands. These measurements improve the accuracy of the wavenumbers previously published and lead to individual absolute line intensities. For retrieving line positions and intensities, a multispectrum fitting procedure [19] has been used to analyze simultaneously five experimental spectra recorded for different pressures of C_2H_2. For each studied band, a vibrational transition dipole moment squared value has been determined, as also empirical Herman-Wallis coefficients. Positions and intensities were then computed for 421 lines from the measured values; a line list containing calculated positions and intensities has been generated for the five strongest bands.

The experimental procedure and the methodology of the analysis will be first presented in Sections 2 and 3 respectively. Then, in Section 4, measured absolute line

positions and intensities will be presented as well as the vibrational transition dipole moments squared and the empirical Herman-Wallis coefficients. A complete line list generated for the whole 3.8-μm spectral region will be described in Appendix.

2. Experimental procedure

For recording the spectra, the rapid scan Bruker IFS 120 HR interferometer of the LADIR (Paris) was used. The unapodized spectral resolution used for each spectrum was equal to 1.1×10^{-3} cm^{-1} (FWHM) and corresponds to a maximal optical path difference of 450 cm. The interferometer was equipped with a CaF$_2$ beam splitter, an InSb detector, a Globar source, and an optical filter covering the 2100 - 3500 cm^{-1} spectral region. The bandpath of the filter has been chosen quite wide allowing the simultaneous recording of three different regions of the acetylene spectrum: around 3 μm, 3.8 μm, and 5 μm. It can be noticed that the 3.8-μm spectral is located in the middle of the filter's response curve (see Fig. 1). Five spectra have been recorded with various C$_2$H$_2$ pressures; experimental conditions are summarized in Table 1. The whole optical path was under vacuum and a multipass cell of one meter base length was used for a total absorption path of 415 ± 1 cm. The cell was equipped with KCl windows. The commercial gas sample, furnished by Air Liquide Alphagaz, with a stated purity of 99.70 % in natural abundances, was used without further purification. The temperature of the gas in the cell was recorded via four platinum probes at different places in the cell. The uncertainty on the temperature measurements has been estimated to be $\pm$ 1 K. The pressure of the gas was measured with a capacitive MKS Baratron manometer with an accuracy estimated to be equal to $\pm$ 1%. Every scan among the 200 recorded for every spectrum has then been individually transformed to spectrum using the Fourier transform procedure included in the Bruker software OPUS package [20], selecting a Mertz phase error correction [21, 22]. The phase error determined by the OPUS software was slightly linear with respect to wavenumbers on the whole spectral region as it has been observed in Ref. [3] when the phase error was obtained using non symmetric apparatus function [23]. In order to obtain a signal to noise ratio nearly equal to 100, the final spectrum was obtained by averaging the Fourier transforms of all the interferograms. Symmetric line profiles were observed on the average spectrum, validating that the phase error was quite well corrected.

3. Line parameters measurements

3.1. The multispectrum fitting procedure

In previous works, line parameters have been retrieved with the aid of a nonlinear least-squares method that adjusts a calculated spectrum to the experimental one [24]. In this work, a multispectrum version [19] of this method was used. We call multispectrum fitting procedure a non linear least-squares method in which several laboratory spectra are analyzed simultaneously, that is to say that correlations between spectra were taken into account, since some of the adjusted line parameters were the same for all the spectra. Line positions (in cm^{-1}), and intensities (in cm/molecule for pure $^{12}C_2H_2$) were obtained in one simultaneous fit of lines belonging to spectra recorded with various experimental conditions. In this work, the absorption path length was fixed to 415 cm but the pressure of C_2H_2 in the cell was varied from 0.5 to 6.8 mbar (see Table 1). At 296 K and 2600 cm^{-1}, the Doppler half-width at half maximum (HWHM) is equal to 0.0026 cm^{-1} for $^{12}C_2H_2$. According to Refs. [25,26] the self-broadening coefficients for $^{12}C_2H_2$ transitions are linearly $|m|$ dependent (m equal $–J$ in P-branch, J in Q-branch, and $J+1$ in R-branch) with no vibrational dependence for the ν_5^1 and the $3\nu_5^1$ band. Taking into account the low pressures used, and the strongest values of broadening coefficients around 0.2 cm^{-1}.atm^{-1}, the collisional half width at half maximum (equal to the product: self-broadening coefficient $\times$ partial pressure of $^{12}C_2H_2$) does not exceed 0.0014 cm^{-1}. The collisional width is not negligible as compared with the Doppler width but is not enough significant to set the self broadening coefficient as an adjustable parameter in the multispectrum fitting. Therefore the broadening coefficients have been constrained to the values obtained in Ref. [4], i.e., same values as in the HITRAN database. Finally, during the simultaneous fit of the five experimental spectra, the line parameters fitted are the line positions and intensities whereas the profile of the line is calculated using a Voigt function. Due to the low pressures, the pressure shift of the lines has been neglected (around $–6\times10^{-5}$ cm^{-1} for the 6.8 mbar pressure spectrum considering the values of self-shifting coefficients obtained in Ref. [4]). The line intensity obtained with the multispectrum procedure is for 296 K for a gas of pure $^{12}C_2H_2$. The line intensity at 296 K is obtained from experimental spectra recorded at temperatures slightly different from 296 K using, for the temperature conversion, the total partition function of Ref. [27].

To retrieve line parameters, the multispectrum procedure has been run with the 5 experimental spectra fitted all together, except for the strongest Q branch of the $\nu_2 + \nu_5^1$ cold

band for which we used only four experimental spectra because the lines in the higher pressure spectrum were saturated. Fig. 2 is a convincing example of the multispectrum fitting procedure efficiency: the whole Q branch of the $\nu_2 + \nu_5^1$ cold band is fitted in one time (J from 1 to 25) in 4 experimental spectra. Line positions and intensities are then obtained for the 25 lines from one simultaneous fit.

During this work, codes of another multispectrum fitting procedure were written in Tomsk. Theses codes, issued from those of Paris, have the same general structure. In Tomsk, the Levenberg-Marquardt algorithm was used to perform the least squares fits, instead of a derivative-free Gauss-Newton algorithm used in Paris. The procedures were cross-validated on usually encountered situations. For that, intensities of a representative sample of lines were measured both in Tomsk and Paris, and were then compared. No significant systematic discrepancy between the two sets of results has been found. The average difference of line intensities Tomsk − Paris is equal to (0.05 ± 1.50) %. The slight dispersion (1 SD) is due to small differences in the treatment of the lines by the two teams (noise operator).

3.2. Preliminaries

3.2.1. Apparatus function and numerical treatment of the spectra

The spectra were not numerically apodized. They were slightly over sampled (over sampling ratio: 2) by post-zero filling the interferograms, but no additional interpolation was performed.

For each spectrum, the apparatus function was calculated [1] performing numerically the Fourier transform of the optical weighting function of the interferogram, due to the throughput, truncated at the maximum optical path difference. To avoid distortion effects, an apparatus function was calculated for each studied line, in order to take into account the wavenumber dependence of the optical weighting [1].

In the definition of the apparatus function, the aperture and the focal length of the collimator are sensitive parameters: nominal values of the aperture (0.4 mm) and of the focal length (418 mm) were used. Due to the small value of the aperture, it was not necessary to determine the effective value of the aperture, contrary to what was done in previous works [3,5,19].

A symmetric apparatus function, was used since, as said in Section 2, the interferograms have been symmetrized using the Mertz method. Comparisons were

performed for several lines to check that same line parameters were found when treating spectra coming from interferograms corrected with the Mertz method, or when analyzing spectra coming directly from non-symmetrized interferograms, but taking into account a phase error through an asymmetric apparatus function (see previous works as Refs. [3,5,19]).

Other miscellaneous considerations have to be pointed out. The zero transmission level was checked using the top of saturated lines present in the 3-μm spectral region of the spectra. No correction was necessary, and it can be assumed that the uncertainty in the transmission scale does not exceed 1%. Furthermore, two weak multiplicative channels, due to the cell windows and to the optical filter, were observed. The first one has a period around 0.25 cm^{-1} with a maximum peak to peak amplitude about 1 %, the second with a period around 3.8 cm^{-1} with a maximum peak to peak amplitude about 2-3%. In the worst case, the effects of these two multiplicative channels do not exceed 1 % on the determination of the continuous background, since the adjusted spectral domains used are always less than the half-period of the strongest channel (and can be reproduced by the adjusted background (see Ref. [19])).

3.2.2. Wavenumbers calibration

In the multispectrum fitting procedure, the absolute zero pressure line positions are the parameters that are looked for (considering the line pressure-shifts negligible). This is possible only if the wavenumber scale of the spectra can be calibrated with respect to standard wavenumbers. In the present work, we calibrated the wavenumbers scale using the line positions of CO_2 present as traces in the tank of the interferometer. The HITRAN wavenumber values [13] were taken as etalon. The quantity $\varepsilon = (\nu_{HITRAN2004} - \nu_{this\ work}) / \nu_{HITRAN2004}$ has been calculated in each spectrum for around 30 transitions belonging to P and R branches of the ν_3 band of $^{12}C^{16}O_2$. These lines were adjusted for each spectrum individually. A very good consistency between the five spectra was found as can be seen in Fig. 3. Averaging the ε quantity for all lines in each spectrum, the mean value 1.285×10^{-6} has been found with a scattering (1SD) smaller than 0.03×10^{-6}, which corresponds to a deviation of 3.33×10^{-3} cm^{-1} at 2600 cm^{-1} and to a scattering (1SD) of 0.06×10^{-3} cm^{-1}. Considering the dispersion of the wavenumber calibration, and the accuracy of the line positions of the ν_3 band of $^{12}C^{16}O_2$ given by HITRAN [13], the accuracy of the wavenumber calibration has been estimated to be better than 0.2×10^{-3} cm^{-1}.

3.2.3. Check of acetylene pressure in the cell

To check the acetylene concentration of the gas sample, line intensities of the cold band $3\nu_5^1$ observed in the 2100 - 2250 cm^{-1} spectral region have been studied and compared with the line intensities published by Jacquemart et al. for this band [3]. To retrieve line intensities for the $3\nu_5^1$ band, the five experimental spectra (see Table 1) have been simultaneously fitted using the multispectrum procedure. The line intensities thus obtained have been gathered in Table 2 together with the values of Ref. [3]. A very good consistency of -0.1 ± 1.2 (1 SD) % was found between our results and those of Ref. [3], and no systematic distortion of the differences is observed with respect to the line position and intensity. Such a small discrepancy shows that the pressure of acetylene in the cell is well known. We estimated the uncertainty of the acetylene pressure in the cell to be smaller than 1 %. It can be noticed that the results given in this work and in Ref. [3] have been obtained using the same multispectrum procedure, but using spectra recorded with the rapid scan interferometer of the LADIR for this work, and the step by step interferometer build in the LPMAA at Paris for the work of Ref. [3]. The present comparison shows the coherence of the spectra recorded with both interferometers.

4. Results

The whole set of measured line positions and intensities is given in Tables 3-8 for the five strongest bands around 3.8 μm, namely the $\nu_2 + \nu_5^1$, $(3\nu_4 + \nu_5)_+^0$, $\nu_1 - \nu_5^1$, $\nu_3 - \nu_4^1$, and $\nu_2 + (\nu_4 + \nu_5)_0^+ - \nu_4^1$ bands. The observed transition dipole moments squared and the calculated line intensities corresponding to the observed line intensities are also reported, as well as the differences between the observed and calculated line positions (only significant parameters have been reported). Let us recall that the self-broadening coefficient has not been determined: this parameter was fixed during the fit (see Section 3.1).

4.1. Line positions

The accurate wavenumber calibration (see section 3.2.2) allowed the determination of absolute line positions, with a mean accuracy of ± 0.0002 cm^{-1}. No attempt has been done in this work to treat theoretically the energy levels; this will be done in a future work in which the resonances will be taken into account through an effective Hamiltonian operator [15-18]. However, to check the assignments and to make some interpolations or extrapolations, line positions have been modeled by empirical polynomial expansions. As they are very effective,

the coefficients obtained for these polynomial expansions are not given here, but a complete list, containing calculated line positions is available upon request. Measured positions and differences between measured and calculated positions are presented in Table 3, 4, 5, 6, and 7 values respectively for the $\nu_2 + \nu_5^1$, $(3\nu_4 + \nu_5)_+^0$, $\nu_1 - \nu_5^1$, $\nu_3 - \nu_4^1$, and $\nu_2 + (\nu_4 + \nu_5)_0^+ - \nu_4^1$ bands. The differences between observed and calculated values are for most of the lines less than 0.0001 cm^{-1}, but can reach 0.0003 cm^{-1} for some transitions corresponding to high J value. In most cases, the differences between measured and calculated positions given in Tables 3-7 are within the mean accuracy of ± 0.0002 cm^{-1} given in this work.

4.2. Line intensities, transition dipole moment squared, and Herman-Wallis factor

The line intensities S_{obs} retrieved from the simultaneous fit of the five experimental spectra are given in cm.molecule^{-1} at 296 K for a pure gas of ^{12}C$_2$H$_2$. The experimental values of line intensities are presented in Tables 3, 4, 5, 6, and 7. In order to check the consistency of the measured values of line intensities, for each transition, the transition dipole moment squared $|R|^2$ (in debye^2) was calculated using the following equation:

$$S_{obs}(T_0) = \frac{1}{4\pi\varepsilon_0} \frac{8\pi^3}{3hc} \frac{\nu_0}{Z_{tot}(T_0)} \exp\left(-\frac{hcE''}{k_BT_0}\right)\left[1 - \exp\left(-\frac{hc\nu_0}{k_BT_0}\right)\right]|R|^2 L(J,\ell)\frac{g_s}{g_l}, \tag{1}$$

where $1/4\pi\varepsilon_0 = 10^{-36}$ erg·cm^3·D^{-2}; h is the Planck's constant equal to 6.6260693(11) $\times 10^{-27}$ erg·s (1 erg = 10^{-7} J); c is the vacuum velocity of light equal to 2.99792458 $\times 10^{10}$ cm·s^{-1}; g_s is the statistical weight due to nuclear spin of the lower level (1 for s-type levels and 3 for a-type levels for ^{12}C$_2$H$_2$); ν_0 is the transition wavenumber in cm^{-1}; g_l is a weight introduced in case of bands with ℓ-type doubling (g_l is equal to 2 when ℓ is greater than 0 for both the upper and lower vibrational levels; otherwise, g_l is equal to 1); $Z_{tot}(T_0)$ is the total partition function at temperature T_0; $L(J,\ell)$ is the Hönl-London factor, J being the rotational quantum number of the lower level of the transition, and ℓ its secondary vibrational quantum number ($\ell = |\ell_4 + \ell_5|$ for C$_2$H$_2$); E'', in cm^{-1}, is the energy of the lower level; k_B is Boltzmann's constant equal to 1.3806505(24) $\times 10^{-16}$ erg·K^{-1}. For the perpendicular bands ($\Delta\ell = \pm 1$) of linear molecules, the Hönl-London factors are given [28] by:

$$L(J,\ell) = (J + 2 + \ell \cdot \Delta\ell)(J + 1 + \ell \cdot \Delta\ell)/[2(J + 1)] \text{ (R-branch)}, \tag{2}$$

$$L(J,\ell) = (J + 1 + \ell \cdot \Delta\ell)(J - \ell \cdot \Delta\ell)(2J + 1)/[2J(J + 1)] \text{ (Q-branch)}, \tag{3}$$

$$L(J,\ell) = (J-1-\ell\cdot\Delta\ell)(J-\ell\cdot\Delta\ell)/[2J] \quad (P\text{-branch}), \tag{4}$$

and for the parallel bands ($\Delta\ell = 0$), the Hönl-London factors are given [28] by:

$$L(J,\ell) = (J+1+\ell)(J+1-\ell)/(J+1) \quad (R\text{-branch}), \tag{5}$$

$$L(J,\ell) = (J+\ell)(J-\ell)/J \quad (P\text{-branch}). \tag{6}$$

The four strongest bands of the 3.8-µm spectral region, namely the $v_2 + v_5^1$, $v_1 - v_5^1$, $v_3 - v_4^1$, and $v_2 + (v_4 + v_5)_0^+ - v_4^1$ bands, are perpendicular-type bands. These bands present a strong Q branch. Contrary to those bands, the $(3v_4 + v_5)_+^0$ cold band is a parallel-type band, and because the vibrational lower and upper states are Σ type, no Q branch is observed for this band.

Once the squared transition dipole moments $|R|^2_{obs}$ are calculated from the observed line intensities, they are plotted for each branch versus m (m being equal to $-J$ in the P branch, J in the Q branch, and $J+1$ in the R branch). For linear molecule as acetylene, the dependence versus m of the squared transition dipole moment is quite smooth. The squared transition dipole moments $|R|^2_{obs}$ allow to check that no major error has been done in the determination of the line intensities. The determination of the squared transition dipole moments allows to reduce the data: empirical parameters are deduced expanding $|R|^2_{obs}$ to take into account its rotational dependence:

$$|R|^2 = |R_0|^2 F(m) ; \tag{7}$$

$|R_0|^2$ is the vibrational transition dipole moment squared, and $F(m)$ is the empirical Herman-Wallis factor which can be expanded using Herman-Wallis coefficients A_1^{RP}, A_2^{RP}, and A_2^Q in the following expressions of $F(m)$:

For P and R branches:
$$F^{RP}(m) = (1 + A_1^{RP}m + A_2^{RP}m^2)^2. \tag{8}$$

For Q branches:
$$F^Q(m) = \left[1 + A_2^Q m(m+1)\right]^2. \tag{9}$$

The experimental transition dipole moments squared $|R|^2_{obs}$ calculated from the line intensities measured in this work have been fitted using Eqs. (7-9). For each band, the fitted parameters which are the vibrational transition dipole moment squared and the Herman-Wallis coefficients, are given in Table 8, together with the vibrational dipole moments

squared. The calculated values $|R|^2_{calc}$ have been obtained using Eqs. (7-9) with the values of Table 8. The experimental and calculated values of the transition dipole moments squared $|R|^2_{obs}$ and $|R|^2_{calc}$ are presented in Tables 3-7 and in Figs. 4-8.

5. Conclusion

In this work, absolute line positions, and line intensities have been measured for around 250 transitions belonging to 2 cold bands and 3 hot bands, namely the $\nu_2 + \nu_5^1$, $(3\nu_4 + \nu_5)_+^0$, $\nu_1 - \nu_5^1$, $\nu_3 - \nu_4^1$, and $\nu_2 + (\nu_4 + \nu_5)_0^+ - \nu_4^1$ bands of acetylene $^{12}C_2H_2$ in the 3.8 μm spectral region. Vibrational transition dipole moments squared and empirical Herman-Wallis coefficients have been determined for each band, as well as empirical coefficients for wavenumbers. All these coefficients allowed to generate a line list of $^{12}C_2H_2$ transitions for the five bands under study.

Appendix

In order to produce a complete line list, an interpolation of our experimental results for transitions that could not been measured on our spectra has to be done. A same slight extrapolation has also been done for all branches of every band up to J equal 30. Up to J equal 25, we still used the Herman-Wallis coefficients of Table 8 in order to calculate the squared transition dipole moment and the line intensity. Between the J values 26 and 30, we fixed the squared transition dipole moment to the value obtain with J equal 25. For the line positions, we used, when available, the experimental values obtained in this work. When the lines could not been studied, we used the value calculated using a polynomial expansion derived from the experimental positions (see Section 4.1). Because of the uncertainty of extrapolated data, we chose to degrade the uncertainty codes for line positions and intensities calculated after J equal 25. Up to J equal to 25, we used for every band the HITRAN error codes 4 (10^{-4} to 10^{-3} cm^{-1}) and 6 (2-5%) [13] respectively for positions and intensities. Between J equal to 26 and 30, we chose the error codes 3 (10^{-3} to 10^{-2} cm^{-1}) and 4 (10-20%) respectively for positions and intensities. Considering that the vibrational dependence for the air- and self-broadening coefficients is negligible, empirical expansions adjusted to experimental results measured in other spectral regions have been used as described in Section 2.3.3 of Ref. [6]. For these parameters, the error codes have been fixed to 6 (2-5%). As far as their temperature-dependence exponent is concerned, the same rough mean value 0.75 was incorporated for all the lines involved in the 3.8-μm spectral region, as well as for all other C_2H_2 lines in the HITRAN database [6,13]. The error code for the temperature-dependence exponent is 4 corresponding to an uncertainty range between 10 and 20%. Finally, in absence of experimental results for air-pressure shifts in the 3.8-μm spectral region, we used, only as a rough estimation, the mean value –0.001 cm^{-1}atm^{-1} obtained for lines in the 5-μm spectral region [4]. Associated to this rough value, we put an error code of 3, corresponding to an uncertainty greater than 20%.

Finally, using a format close to those of HITRAN [13], we created a complete line list up to J equal to 30 for the five bands studied in this work, namely the $\nu_2 + \nu_5^1$ and $(3\nu_4 + \nu_5)_+^0$ cold bands, and the $\nu_1 - \nu_5^1$, $\nu_3 - \nu_4^1$, and $\nu_2 + (\nu_4 + \nu_5)_0^+ - \nu_4^1$ hot bands. This line list contains 421 lines and is available upon requests to the authors. We will propose it to be added to the HITRAN and GEISA databases. An extract of this line list is presented in Table 9.

References

[1] Mandin JY, Dana V, Claveau C. Line intensities in the ν_5 band of acetylene $^{12}C_2H_2$. JQSRT 2000;67:429-46.

[2] Jacquemart D, Claveau C, Mandin JY, Dana V. Line intensities of hot bands in the 13.6 μm spectral region of acetylene $^{12}C_2H_2$. JQSRT 2001;69:81-101.

[3] Jacquemart D, Mandin JY, Dana V, Régalia-Jarlot L, Thomas X, Von Der Heyden. Multispectrum fitting measurements of line parameters for 5 μm cold bands of acetylene. JQSRT 2002;75:397-422.

[4] Jacquemart D, Mandin JY, Dana V, Régalia-Jarlot L, Plateaux JJ, Décatoire D, Rothman LS. The spectrum of acetylene in the 5μm region from new line parameter measurements. JQSRT 2003;76:237-67.

[5] Mandin JY, Jacquemart D, Dana V, Régalia-Jarlot L, Barbe A. Line intensities of acetylene at 3 μm. JQSRT 2005;92:239-60.

[6] Jacquemart D, Mandin JY, Dana V, Claveau C, Vander Auwera J, Herman M, Rothman LS, Régalia-Jarlot L, Barbe A. The IR acetylene spectrum in HITRAN: update and new results. JQSRT 2003;82:363-82.

[7] Wiggins TA, Plyler EK, Tidwell ED. Infrared spectrum of acetylene. J Opt Soc Amer 1961;51:1219-25.

[8] Palmer KF, Mickelson ME, Rao KN. Investigations of several infrared bands of $^{12}C_2H_2$ and studies of the effects of vibrational rotational interactions. J Mol Spectrosc 1972;44:131-44.

[9] Plíva J. Spectrum of acetylene in the 5-micron region. J Mol Spectrosc 1972;44:145-64.

[10] D'Cunha R, Sarma YA., Job VA., Guelachvili G, Rao KN. Fermi coupling and l-type resonance effects in the hot bands of acetylene: the 2650-cm^{-1} region. J Mol Spectrosc 1993;157:358-68.

[11] Koops Th, Smit WMA, Visser T. Measurement and interpretation of the absolute infrared intensities of acetylene: fundamentals and combination bands. J Mol Struct 1984;112:285-99.

[12] Rinsland CP, Baldacci A, Rao KN. Acetylene bands observed carbon stars: a laboratory study and an illustrative example of its application to IRC+10216. APJ Sup Series 1982;49:487-513.

[13] Rothman LS, Jacquemart D, Barbe A, Benner DC, Birk M, Brown LR, Carleer MR, Chackerian Jr C, Chance K, Coudert LH, Dana V, Devi VM, Flaud JM, Gamache RR, Goldman A, Hartmann JM, Jucks KW, Maki AG, Mandin JY, Massie ST, Orphal J, Perrin A, Rinsland CP, Smith MAH, Tennyson J, Tolchenov RN, Toth RA, Vander Auwera J, Varanasi P, Wagner G. The HITRAN 2004 molecular spectroscopic database. JQSRT 2005;96:139-204.

[14] Jacquinet-Husson N, Scott NA, Chedin A, Garceran K, Armante R, Chursin AA, Barbe A, Birk M, Brown LR, Camy-Peyret C, Claveau C, Clerbaux C, Coheur PF, Dana V, Daumont L, Debacker-Barilly MR, Flaud JM, Goldman A, Hamdouni A, Hess M, Jacquemart D, Köpke P, Mandin JY, Massie S, Mikhailenko S, Nemtchinov V, Nikitin A, Newnham D, Perrin A, Perevalov VI, Régalia-Jarlot L, Rublev A, Schreier F, Schult I, Smith KM, Tashkun SA, Teffo JL, Toth RA, Tyuterev VIG, Vander Auwera J, Varanasi P, Wagner G. The 2003 Edition Of The GEISA/IASI spectroscopic database. JQSRT 2005;95:429-67.

[15] Perevalov VI, Lyulin OM, Jacquemart D, Claveau C, Teffo JL, Dana V, Mandin JY, Valentin A. Global fitting of line intensities of acetylene molecule in the infrared using the effective operator approach. J Mol Spectrosc 2003;218:180-9.

[16] Lyulin OM, Perevalov VI, Tashkun SA, Teffo JL. Global fitting of the vibrational-rotational line positions of acetylene molecule in the far and middle infrared regions. In: Proceedings of the XIVth Symposium on High-Resolution Molecular Spectroscopy, Krosnoyarsk, Russia. SPIE 2004;5311:134-43.

[17] Lyulin OM, Perevalov VI, Mandin JY, Dana V, Jacquemart D, Regalia-Jarlot L, Barbe A. Line intensities of acetylene in the 3-mm region: New measurements of weak hot bands and global fitting. JQSRT 2006;97:81-98.

[18] Perevalov VI, Lobodenko EI, Teffo JL. Reduced effective Hamiltonian for global fitting of C_2H_2 rovibrational lines. In:Proceedings of the XIIth symposium and school on high-resolution molecular spectroscopy, St. Petersburg:SPIE 1997;3090: 143–9.

[19] Jacquemart D, Mandin JY, Dana V, Picqué N, Guelachvili G. A multispectrum fitting procedure to deduce molecular line parameters. Application to the 3-0 band of $^{12}C^{16}O$. Eur Phys J D 2001;14:55-69.

[20] Wartewig S. IR and Raman Spectroscopy: Fundamental Processing. Wiley-VCH, Weinheim, 2003.

[21] Mertz L. Transformations in Optics. Wiley, New York, 1965.

[22] Griffiths PR, deHaseth JA. Fourier Transform Infrared Spectrometry. Wiley, New York, 1986.

[23] Dana V, Mandin JY, Hamdouni A. Phase errors on interferograms: influence on the determination of positions, intensities, and widths of lines in the infrared. Appl Opt 1992;31:1937-41.

[24] Dana V, Mandin JY. New improvements in the determination of line parameters from FTS data. JQSRT 1992;48:725-31.

[25] Lambot D. Étude de l'élargissement collisionnel de raies d'absorption infrarouge en phase gazeuse: application à la bande ν_5 de C_2H_2. Thèse en Sciences, Facultés Universitaires Notre-Dame de la Paix, Namur, Belgium, 1993.

[26] Jacquemart D. Développement d'une procédure d'ajustement simultané de plusieurs spectres obtenus par transformation de Fourier. Détermination des paramètres de raies de l'acétylène dans les régions à 5 μm et 13,6 μm. Thèse en Spectroscopie moléculaire, Université Pierre et Marie Curie, Paris, France, 2002.

[27] Gamache RR, Kennedy S, Hawkins RL, Rothman LS. Total internal partition sums for molecules in the terrestrial atmosphere. J Mol Struct 2000;517-8:407-25.

[28] Rothman LS, Hawkins RL, Wattson RB, Gamache RR. Energy levels, intensities, and linewidths of atmospheric carbon dioxide bands. JQSRT 1992;48:537-66.

Captions of tables

Table 1. Experimental conditions and characteristics of the recorded spectra

Table 2.   Comparisons between line intensities obtained by Jacquemart et al. [3] and obtained in this work for the $3\nu_5^1$ band of $^{12}C_2H_2$ [a]

[a] The line positions, in cm^{-1}, are from Ref. [3]. S_{obs} are measured line intensities in $cm^{-1}/(molecule·cm^{-2})$ at 296 K for pure $^{12}C_2H_2$. % is $100 \times (S_{obs}$ [3] $- S_{obs}$ (this work)) $/ S_{obs}$ [3].

Table 3. Line parameters obtained for the $\nu_2 + \nu_5^1$ band of $^{12}C_2H_2$ [a]

[a]   The lines are given by increasing wavenumber inside each branch. In the Line column, the first quoted character e or f concerns the upper level, and the second the lower level. The position column contains the measured line position in cm^{-1} and Dif is the difference in 10^{-3} cm^{-1} between the measured position and the one calculated using a polynomial expansion. S_{obs} is the measured line intensity in $cm·molecule^{-1}$, for pure $^{12}C_2H_2$ at 296 K, and S_{calc} the one calculated (see text) using the constants of Table 8 (see Eqs. 1-9). % is the percentage ratio $100 \times (S_{obs} - S_{calc}) / S_{obs}$. $|R|_{obs}^2$ is the transition dipole moment squared in D^2 (1 D = 3.33546×10^{-30} C·m) deduced from S_{obs}.

Table 4. Line parameters obtained for the $(3\nu_4 + \nu_5)_+^0$ band of $^{12}C_2H_2$ [a]

[a] See footnote of Table 3 for the meaning of column headings.

Table 5. Line parameters obtained for the $\nu_1 - \nu_5^1$ band of $^{12}C_2H_2$ [a]

[a] See footnote of Table 3 for the meaning of column headings.

Table 6. Line parameters obtained for the $\nu_3 - \nu_4^1$ band of $^{12}C_2H_2$ [a]

[a] See footnote of Table 3 for the meaning of column headings.

Table 7. Line parameters obtained for the $\nu_2 + (\nu_4 + \nu_5)_0^+ - \nu_4^1$ band of $^{12}C_2H_2$ [a]

[a] See footnote of Table 3 for the meaning of column headings.

Table 8.   Summary of $^{12}C_2H_2$ vibrational transition dipole moments squared, and Herman-Wallis coefficients, obtained for the 5 bands analyzed in this work (see Eqs. (1-9))

Table 9. Extract of the line list of $^{12}C_2H_2$ around 3.8 μm

Captions of figures

Fig. 1. Overview of the 5 spectra recorded in this work with the Bruker IFS 120 interferometer of the LADIR. We assigned a number from 1 to 5 to these experimental spectra (see Table 1 for details). Four spectral regions of noticeable absorption are observed: around 2200 cm^{-1} where one can see the $3\nu_5^1$ band of ^{12}C$_2$H$_2$ used to check the purity of the gas (see text); around 2350 cm^{-1} where the absorption of the strong ν_3 band of ^{12}C^{16}O$_2$ (used for the wavenumber calibration, see text) is due to small traces of this gas in the sample; around 2700 cm^{-1} where one can see the 5 strongest bands of ^{12}C$_2$H$_2$ studied in this work; and finally the strong absorption of numerous bands of ^{12}C$_2$H$_2$ around 3300 cm^{-1}.

Fig. 2. This figure represents the whole Q_{fe} branch of the $\nu_2 + \nu_5^1$ band observed in 4 experimental spectra recorded in this work (numbers 1-4, see Table 1), and the difference (noted obs–calc) between these experimental spectra and those which are simultaneously adjusted with the multispectrum fitting procedure. The spectral domain adjusted during the fit is equal to 1.4 cm^{-1}, so that all the lines of the whole Q branch were fitted simultaneously in the 4 spectra together.

Fig. 3. Wavenumber calibration factor $\varepsilon = (\nu_{\text{HITRAN2004}} - \nu_{\text{this work}}) / \nu_{\text{HITRAN2004}}$ obtained for transitions of the ν_3 band of ^{12}C^{16}O$_2$ in the 5 experimental spectra of this work. The straight line represents the average value $\langle \varepsilon \rangle = 1.285(32) \times 10^{-6}$ which means a shift of $3.33(6) \times 10^{-3}$ cm^{-1} at 2600 cm^{-1} (numbers of the spectra refer to those of Table 1).

Fig.4. Experimental and calculated values of the transition dipole moment squared of the $\nu_2 + \nu_5^1$ band. Black triangles are for P_{ee} and R_{ee} lines, and black squares for Q_{fe} lines. The curves have been calculated using the constants found in this work (see Table 8).

Fig.5. Experimental and calculated values of the transition dipole moment squared of the $(3\nu_4 + \nu_5)_0^+$ band. Black triangles are for P_{ee} and R_{ee} lines. The curves have been calculated using the constants found in this work (see Table 8).

Fig.6. Experimental and calculated values of the transition dipole moment squared of the $\nu_1 - \nu_5^1$ band. Black triangles are for P_{ee} and R_{ee} lines, and black squares for Q_{ef} lines. The curves have been calculated using the constants found in this work (see Table 8).

Fig.7. Experimental and calculated values of the transition dipole moment squared of the $\nu_3 - \nu_4^1$ band. Black triangles are for P_{ee} and R_{ee} lines, and black squares for Q_{ef} lines. The curves have been calculated using the constants found in this work (see Table 8).

Fig.8. Experimental and calculated values of the transition dipole moment squared of the $\nu_2 + (\nu_4 + \nu_5)_0^+ - \nu_4^1$ band. Black triangles are for P_{ee} and R_{ee} lines, and black squares for Q_{ef} lines. The curves have been calculated using the constants found in this work (see Table 8).

Table 1. Experimental conditions and characteristics of the recorded spectra

Unapodized *apparatus function*
Maximum optical path difference   450 cm
FWHM $\approx 1.1 \times 10^{-3} \text{ cm}^{-1}$
Iris radius   0.4 mm
Collimator focal length   418 mm

Absorbing sample
Natural C_2H_2 97.760 % of $^{12}C_2H_2$
Stated purity   99.70 %

Experimental conditions
SNR ≈ 100
Absorption path   415 cm

#	Total pressure (mbar) [a]	Temperature (K)
1	0.497	297.6_5
2	1.48_0	298.1_5
3	2.51_0	297.1_5
4	4.03_4	297.9_5
5	6.83_3	297.1_5

[a] 1 atm = 1013 mbar = 1013 hPa.

Table 2. Comparisons between line intensities obtained by Jacquemart et al. [3] and obtained in this work for the $3\nu_5^1$ band of $^{12}C_2H_2$ [a]

Line	Position	S_{obs} [3]	S_{obs} (this work)	%
P 25	2111.3198	2.18E-23	2.17E-23	0.5
P 23	2115.8994	3.49E-23	3.49E-23	0.0
P 22	2118.1899	1.43E-23	1.46E-23	-2.1
P 21	2120.4811	5.26E-23	5.24E-23	0.4
P 20	2122.7734	2.10E-23	2.10E-23	0.0
P 18	2127.3619	2.94E-23	2.92E-23	0.7
P 17	2129.6586	1.03E-22	1.01E-22	2.0
P 14	2136.5613	4.73E-23	4.74E-23	-0.2
P 13	2138.8672	1.54E-22	1.55E-22	-0.6
P 11	2143.4877	1.71E-22	1.70E-22	0.6
P 6	2155.0977	4.73E-23	4.77E-23	-0.8
P 2	2164.4545	1.14E-23	1.17E-23	-2.6
R 8	2190.5039	7.68E-23	7.67E-23	0.1
R 10	2195.2817	7.34E-23	7.40E-23	-0.8
R 11	2197.6740	2.11E-22	2.09E-22	1.0
R 12	2200.0680	6.56E-23	6.54E-23	0.3
R 13	2202.4638	1.82E-22	1.80E-22	1.1
R 14	2204.8607	5.48E-23	5.50E-23	-0.4
R 15	2207.2586	1.47E-22	1.46E-22	0.7
R 16	2209.6572	4.29E-23	4.22E-23	1.7
R 17	2212.0562	1.12E-22	1.12E-22	0.0
R 18	2214.4551	3.18E-23	3.16E-23	0.6
R 19	2216.8539	8.18E-23	8.07E-23	1.4
R 20	2219.2519	2.23E-23	2.20E-23	1.4
R 25	2231.2229	2.15E-23	2.17E-23	-0.9
R 27	2235.9968	1.24E-23	1.27E-23	-2.4

[a] The line positions, in cm^{-1}, are from Ref. [3]. S_{obs} are measured line intensities in cm^{-1}/(molecule·cm^{-2}) at 296 K for pure $^{12}C_2H_2$. % is $100 \times (S_{obs}$ [3] $- S_{obs}$ (this work)) / S_{obs} [3].

Table 3. Line parameters obtained for the $\nu_2 + \nu_5^1$ band of $^{12}C_2H_2$ [a]

Line	Position	Dif	S_{obs}	S_{calc}	%	$|R|^2_{obs}$
Pee21	2649.84412	0.27	1.05E-22	1.02E-22	2.9	1.84E-05
Pee19	2655.03773	0.01	1.49E-22	1.51E-22	-1.3	1.80E-05
Pee18	2657.61640	-0.01	5.87E-23	5.98E-23	-1.9	1.82E-05
Pee17	2660.18288	0.01	2.07E-22	2.10E-22	-1.4	1.84E-05
Pee16	2662.73710	0.01	8.05E-23	8.08E-23	-0.4	1.89E-05
Pee15	2665.27904	0.01	2.72E-22	2.75E-22	-1.1	1.90E-05
Pee14	2667.80859	-0.05	1.01E-22	1.02E-22	-1.0	1.92E-05
Pee13	2670.32593	0.03	3.34E-22	3.37E-22	-0.9	1.95E-05
Pee12	2672.83080	0.02	1.21E-22	1.21E-22	0.0	1.99E-05
Pee10	2677.80319	-0.03	1.33E-22	1.32E-22	0.8	2.06E-05
Pee 9	2680.27075	0.04	4.00E-22	4.00E-22	0.0	2.06E-05
Pee 6	2687.59777	-0.05	1.16E-22	1.14E-22	1.7	2.17E-05
Pee 4	2692.41934	-0.02	7.87E-23	7.94E-23	-0.9	2.17E-05
Pee 2	2697.19006	0.06	2.91E-23	2.94E-23	-1.0	2.22E-05
Qfe25	2700.75509	-0.01	1.17E-22	1.16E-22	0.9	2.30E-05
Qfe24	2700.84542	0.12	4.86E-23	4.95E-23	-1.9	2.24E-05
Qfe23	2700.93160	-0.06	1.85E-22	1.87E-22	-1.1	2.25E-05
Qfe22	2701.01412	-0.11	7.74E-23	7.78E-23	-0.5	2.27E-05
Qfe21	2701.09298	-0.04	2.83E-22	2.87E-22	-1.4	2.26E-05
Qfe20	2701.16793	-0.13	1.15E-22	1.16E-22	-0.9	2.27E-05
Qfe19	2701.23947	0.09	4.13E-22	4.15E-22	-0.5	2.27E-05
Qfe18	2701.30709	0.11	1.62E-22	1.63E-22	-0.6	2.28E-05
Qfe17	2701.37106	0.15	5.63E-22	5.69E-22	-1.1	2.26E-05
Qfe16	2701.43112	-0.06	2.14E-22	2.17E-22	-1.4	2.26E-05
Qfe15	2701.48776	-0.04	7.27E-22	7.35E-22	-1.1	2.26E-05
Qfe14	2701.54074	-0.06	2.71E-22	2.72E-22	-0.4	2.28E-05
Qfe13	2701.59030	0.12	8.82E-22	8.91E-22	-1.0	2.26E-05
Qfe12	2701.63595	-0.01	3.15E-22	3.19E-22	-1.3	2.26E-05
Qfe11	2701.67819	0.01	1.02E-21	1.01E-21	1.0	2.31E-05
Qfe10	2701.71676	-0.07	3.45E-22	3.49E-22	-1.2	2.26E-05
Qfe 9	2701.75192	0.00	1.06E-21	1.06E-21	0.0	2.28E-05
Qfe 8	2701.78341	-0.07	3.51E-22	3.51E-22	0.0	2.29E-05
Qfe 7	2701.81149	-0.02	1.02E-21	1.02E-21	0.0	2.29E-05
Qfe 6	2701.83590	-0.10	3.20E-22	3.19E-22	0.3	2.29E-05
Qfe 5	2701.85714	0.16	8.68E-22	8.66E-22	0.2	2.29E-05
Qfe 4	2701.87448	0.01	2.51E-22	2.50E-22	0.4	2.29E-05
Qfe 3	2701.88839	-0.05	6.16E-22	6.11E-22	0.8	2.30E-05
Qfe 2	2701.89889	-0.03	1.63E-22	1.51E-22	7.4	2.47E-05
Qfe 1	2701.90597	0.07	2.87E-22	2.77E-22	3.5	2.37E-05
Ree 0	2704.24986	0.04	6.29E-23	6.31E-23	-0.3	2.30E-05
Ree 1	2706.57724	-0.05	2.91E-22	2.84E-22	2.4	2.39E-05
Ree 2	2708.89180	-0.02	1.26E-22	1.25E-22	0.8	2.38E-05
Ree 3	2711.19334	0.00	4.58E-22	4.58E-22	0.0	2.39E-05
Ree 4	2713.48182	-0.01	1.79E-22	1.77E-22	1.1	2.44E-05
Ree 5	2715.75725	0.02	5.91E-22	5.92E-22	-0.2	2.44E-05
Ree 6	2718.01951	0.00	2.14E-22	2.13E-22	0.5	2.48E-05
Ree 8	2722.50456	0.00	2.30E-22	2.29E-22	0.4	2.53E-05
Ree 9	2724.72725	0.01	6.93E-22	6.91E-22	0.3	2.56E-05
Ree10	2726.93664	0.01	2.27E-22	2.27E-22	0.0	2.58E-05
Ree11	2729.13271	0.00	6.57E-22	6.57E-22	0.0	2.60E-05
Ree12	2731.31541	-0.01	2.08E-22	2.08E-22	0.0	2.64E-05
Ree13	2733.48470	-0.02	5.91E-22	5.82E-22	1.5	2.70E-05
Ree14	2735.64058	0.01	1.79E-22	1.78E-22	0.6	2.69E-05
Ree15	2737.78296	0.02	4.84E-22	4.84E-22	0.0	2.71E-05
Ree16	2739.91175	-0.02	1.43E-22	1.44E-22	-0.7	2.72E-05
Ree17	2742.02704	0.01	3.78E-22	3.79E-22	-0.3	2.75E-05
Ree18	2744.12866	0.00	1.09E-22	1.09E-22	0.0	2.78E-05
Ree19	2746.21668	0.02	2.79E-22	2.81E-22	-0.7	2.80E-05
Ree20	2748.29093	-0.02	7.86E-23	7.88E-23	-0.3	2.84E-05

```
Ree21   2750.35150   0.00     1.95E-22 1.97E-22   -1.0     2.86E-05
Ree22   2752.39830   0.01     5.32E-23 5.37E-23   -0.9     2.88E-05
```

[a] The lines are given by increasing wavenumber inside each branch. In the Line column, the first quoted character e or f concerns the upper level, and the second the lower level. The position column contains the measured line position in cm^{-1} and Dif is the difference in 10^{-3} cm^{-1} between the measured position and the one calculated using a polynomial expansion. S_{obs} is the measured line intensity in cm·molecule^{-1}, for pure $^{12}C_2H_2$ at 296 K, and S_{calc} the one calculated (see text) using the constants of Table 8 (see Eqs. 1-9). % is the percentage ratio $100 \times (S_{obs} - S_{calc}) / S_{obs}$. $|R|^2_{obs}$ is the transition dipole moment squared in D^2 (1 D = 3.33546×10^{-30} C·m) deduced from S_{obs}.

Table 4. Line parameters obtained for the $(3\nu_4 + \nu_5)_0^+$ cold band of $^{12}C_2H_2$ [a]

Line	Position	Dif	S_{obs}	S_{calc}	%	$|R|^2_{obs}$
Pee21	2515.45775	0.40	1.47E-23	1.46E-23	0.7	1.29E-06
Pee20	2517.34052	-0.54	6.25E-24	6.08E-24	2.7	1.36E-06
Pee19	2519.25092	-0.38	2.28E-23	2.24E-23	1.8	1.38E-06
Pee18	2521.18952	-0.05	8.99E-24	9.04E-24	-0.6	1.39E-06
Pee17	2523.15750	0.40	3.23E-23	3.23E-23	0.0	1.43E-06
Pee16	2525.15543	0.76	1.25E-23	1.26E-23	-0.8	1.45E-06
Pee14	2529.24121	0.04	1.69E-23	1.64E-23	3.0	1.57E-06
Pee12	2533.44672	-0.53	2.04E-23	1.98E-23	2.9	1.63E-06
Pee11	2535.59234	-0.58	6.53E-23	6.36E-23	2.6	1.64E-06
Pee10	2537.76478	-0.41	2.20E-23	2.22E-23	-0.9	1.61E-06
Pee 9	2539.96240	-0.08	6.95E-23	6.80E-23	2.2	1.68E-06
Pee 8	2542.18330	0.25	2.32E-23	2.26E-23	2.6	1.70E-06
Pee 7	2544.42558	0.43	6.69E-23	6.57E-23	1.8	1.71E-06
Pee 6	2546.68758	0.56	2.13E-23	2.05E-23	3.8	1.76E-06
Pee 5	2548.96744	0.41	5.55E-23	5.54E-23	0.2	1.71E-06
Pee 4	2551.26388	0.21	1.59E-23	1.58E-23	0.6	1.73E-06
Pee 3	2553.57558	-0.10	3.77E-23	3.73E-23	1.1	1.74E-06
Pee 2	2555.90185	-0.21	8.38E-24	8.61E-24	-2.7	1.68E-06
Pee 1	2558.24165	-0.45	1.29E-23	1.33E-23	-3.1	1.69E-06
Ree 0	2562.96124	-0.72	4.32E-24	4.48E-24	-3.7	1.67E-06
Ree 1	2565.34175	-0.28	2.60E-23	2.65E-23	-1.9	1.69E-06
Ree 2	2567.73628	0.03	1.25E-23	1.29E-23	-3.2	1.66E-06
Ree 3	2570.14589	0.33	4.96E-23	4.98E-23	-0.4	1.71E-06
Ree 4	2572.57155	0.42	2.00E-23	1.97E-23	1.5	1.73E-06
Ree 5	2575.01482	0.45	6.64E-23	6.67E-23	-0.5	1.69E-06
Ree 8	2582.46613	-0.21	2.59E-23	2.56E-23	1.2	1.67E-06
Ree10	2587.55252	-0.33	2.41E-23	2.45E-23	-1.7	1.57E-06
Ree12	2592.74733	-0.43	2.25E-23	2.16E-23	4.0	1.61E-06
Ree14	2598.05871	0.53	1.79E-23	1.77E-23	1.1	1.51E-06
Ree15	2600.75755	0.27	4.63E-23	4.67E-23	-0.9	1.45E-06
Ree16	2603.48495	-0.12	1.31E-23	1.35E-23	-3.1	1.39E-06
Ree17	2606.24018	-0.36	3.30E-23	3.44E-23	-4.2	1.34E-06
Ree18	2609.02245	0.16	9.09E-24	9.61E-24	-5.7	1.28E-06

[a] See footnote of Table 3 for the meaning of column headings.

Table 5. Line parameters obtained for the $\nu_1 - \nu_5^1$ band of $^{12}\text{C}_2\text{H}_2$ [a]

Line	Position	Dif	S_{obs}	S_{calc}	%	$|R|^2_{obs}$
Pee24	2583.65462	0.31	5.74E-23	5.68E-23	1.0	6.26E-04
Pee23	2586.30116	-0.02	2.42E-23	2.38E-23	1.7	6.26E-04
Pee22	2588.93572	0.05	8.91E-23	8.84E-23	0.8	6.16E-04
Pee21	2591.55779	0.01	3.62E-23	3.60E-23	0.6	6.10E-04
Pee20	2594.16745	-0.04	1.31E-22	1.30E-22	0.8	6.04E-04
Pee19	2596.76477	0.02	5.16E-23	5.16E-23	0.0	5.97E-04
Pee18	2599.34956	0.02	1.81E-22	1.82E-22	-0.6	5.92E-04
Pee17	2601.92176	-0.06	6.96E-23	7.00E-23	-0.6	5.86E-04
Pee16	2604.48154	0.01	2.39E-22	2.39E-22	0.0	5.84E-04
Pee15	2607.02863	0.00	9.03E-23	8.96E-23	0.8	5.85E-04
Pee14	2609.56314	0.03	2.96E-22	2.97E-22	-0.3	5.75E-04
Pee11	2617.09018	0.01	1.21E-22	1.21E-22	0.0	5.61E-04
Pee10	2619.57359	0.00	3.74E-22	3.76E-22	-0.5	5.57E-04
Pee 9	2622.04414	-0.01	1.26E-22	1.27E-22	-0.8	5.52E-04
Pee 8	2624.50176	-0.03	3.74E-22	3.78E-22	-1.1	5.46E-04
Pee 7	2626.94647	-0.01	1.20E-22	1.22E-22	-1.7	5.40E-04
Pee 5	2631.79686	0.04	1.04E-22	1.05E-22	-1.0	5.36E-04
Pee 3	2636.59488	0.02	7.58E-23	7.62E-23	-0.5	5.28E-04
Pee 2	2638.97415	-0.02	1.76E-22	1.76E-22	0.0	5.25E-04
Qef24	2636.91066	-0.03	3.07E-23	3.13E-23	-2.0	5.09E-04
Qef22	2637.97074	0.01	4.96E-23	4.93E-23	0.6	5.23E-04
Qef21	2638.46722	-0.02	1.83E-22	1.82E-22	0.5	5.23E-04
Qef20	2638.94139	0.02	7.32E-23	7.35E-23	-0.4	5.17E-04
Qef17	2640.22926	-0.01	3.64E-22	3.62E-22	0.5	5.22E-04
Qef15	2640.97554	0.01	4.68E-22	4.69E-22	-0.2	5.19E-04
Qef14	2641.31490	0.00	1.74E-22	1.74E-22	0.0	5.19E-04
Qef12	2641.92597	-0.03	2.08E-22	2.04E-22	1.9	5.29E-04
Qef11	2642.19773	0.03	6.53E-22	6.47E-22	0.9	5.24E-04
Qef10	2642.44681	-0.01	2.24E-22	2.23E-22	0.4	5.21E-04
Qef 9	2642.67335	0.02	6.81E-22	6.80E-22	0.1	5.20E-04
Qef 8	2642.87726	0.03	2.24E-22	2.25E-22	-0.4	5.18E-04
Qef 7	2643.05850	0.00	6.51E-22	6.53E-22	-0.3	5.18E-04
Qef 6	2643.21713	-0.01	2.04E-22	2.04E-22	0.0	5.19E-04
Qef 5	2643.35312	-0.01	5.53E-22	5.56E-22	-0.5	5.17E-04
Qef 4	2643.46645	-0.01	1.59E-22	1.60E-22	-0.6	5.15E-04
Qef 3	2643.55719	0.05	3.95E-22	3.92E-22	0.8	5.23E-04
Qef 2	2643.62511	-0.04	9.51E-23	9.66E-23	-1.6	5.11E-04
Qef 1	2643.67047	-0.03	1.78E-22	1.78E-22	0.0	5.18E-04
Ree 4	2655.25762	0.00	2.06E-22	2.07E-22	-0.5	4.98E-04
Ree 5	2657.53027	0.00	8.04E-23	8.08E-23	-0.5	4.93E-04
Ree 6	2659.78944	0.01	2.69E-22	2.70E-22	-0.4	4.90E-04
Ree 7	2662.03507	0.03	9.70E-23	9.61E-23	0.9	4.92E-04
Ree 8	2664.26708	0.00	2.98E-22	2.99E-22	-0.3	4.83E-04
Ree 9	2666.48545	-0.04	9.87E-23	1.00E-22	-1.3	4.72E-04
Ree10	2668.69026	-0.01	2.93E-22	2.96E-22	-1.0	4.71E-04
Ree11	2670.88132	-0.03	9.45E-23	9.50E-23	-0.5	4.69E-04
Ree12	2673.05871	0.00	2.68E-22	2.69E-22	-0.4	4.67E-04
Ree14	2677.37221	0.05	2.30E-22	2.27E-22	1.3	4.67E-04
Ree15	2679.50817	0.03	6.78E-23	6.79E-23	-0.1	4.56E-04
Ree16	2681.63029	-0.01	1.81E-22	1.79E-22	1.1	4.57E-04
Ree17	2683.73855	-0.01	5.27E-23	5.20E-23	1.3	4.56E-04
Ree18	2685.83293	0.02	1.33E-22	1.33E-22	0.0	4.44E-04
Ree19	2687.91322	-0.09	3.78E-23	3.75E-23	0.8	4.46E-04
Ree21	2692.03225	0.09	2.58E-23	2.55E-23	1.2	4.38E-04
Ree22	2694.07049	-0.05	6.23E-23	6.19E-23	0.6	4.33E-04

[a] See footnote of Table 3 for the meaning of column headings.

Table 6. Line parameters obtained for the $\nu_3 - \nu_4^1$ band of $^{12}C_2H_2$ [a]

Line	Position	Dif	S_{obs}	S_{calc}	%	$\lvert R \rvert_{obs}^2$
Pee23	2627.33685	-0.24	6.24E-23	6.34E-23	-1.6	2.99E-04
Pee22	2629.86098	-0.01	2.53E-23	2.63E-23	-4.0	2.91E-04
Pee20	2634.87537	0.02	3.84E-23	3.89E-23	-1.3	2.96E-04
Pee19	2637.36639	0.02	1.38E-22	1.39E-22	-0.7	2.96E-04
Pee17	2642.31781	-0.04	1.88E-22	1.90E-22	-1.1	2.94E-04
Pee16	2644.77914	-0.01	7.25E-23	7.24E-23	0.1	2.95E-04
Pee13	2652.11033	0.02	2.98E-22	2.96E-22	0.7	2.93E-04
Pee12	2654.53776	0.01	1.06E-22	1.06E-22	0.0	2.91E-04
Pee11	2656.95766	0.01	3.39E-22	3.36E-22	0.9	2.92E-04
Pee10	2659.37034	0.01	1.16E-22	1.16E-22	0.0	2.88E-04
Pee 9	2661.77607	0.01	3.55E-22	3.53E-22	0.6	2.88E-04
Pee 5	2671.33405	-0.01	2.97E-22	2.95E-22	0.7	2.84E-04
Pee 4	2673.70811	-0.06	8.80E-23	8.64E-23	1.8	2.86E-04
Pee 2	2678.43868	0.01	5.57E-23	5.58E-23	-0.2	2.78E-04
Pee 1	2680.79520	0.05	1.13E-22	1.14E-22	-0.9	2.75E-04
Qef24	2677.79222	-0.11	7.22E-23	7.34E-23	-1.7	2.22E-04
Qef23	2678.25030	-0.04	3.21E-23	3.14E-23	2.2	2.34E-04
Qef22	2678.68528	0.06	1.19E-22	1.19E-22	0.0	2.32E-04
Qef21	2679.09726	0.04	4.94E-23	4.97E-23	-0.6	2.35E-04
Qef20	2679.48664	-0.04	1.87E-22	1.84E-22	1.6	2.44E-04
Qef19	2679.85390	-0.03	7.40E-23	7.42E-23	-0.3	2.42E-04
Qef18	2680.19940	-0.01	2.65E-22	2.66E-22	-0.4	2.46E-04
Qef17	2680.52350	-0.02	1.04E-22	1.04E-22	0.0	2.49E-04
Qef16	2680.82673	0.00	3.62E-22	3.63E-22	-0.3	2.52E-04
Qef15	2681.10949	0.02	1.38E-22	1.38E-22	0.0	2.55E-04
Qef14	2681.37220	0.03	4.63E-22	4.65E-22	-0.4	2.57E-04
Qef13	2681.61532	0.01	1.70E-22	1.71E-22	-0.6	2.58E-04
Qef11	2682.04442	0.02	1.99E-22	1.97E-22	1.0	2.66E-04
Qef10	2682.23115	0.01	6.17E-22	6.18E-22	-0.2	2.66E-04
Qef 9	2682.39976	-0.04	2.12E-22	2.10E-22	0.9	2.70E-04
Qef 8	2682.55070	0.01	6.31E-22	6.30E-22	0.2	2.70E-04
Qef 7	2682.68408	-0.03	2.04E-22	2.04E-22	0.0	2.71E-04
Qef 6	2682.80029	-0.01	5.82E-22	5.78E-22	0.7	2.74E-04
Qef 5	2682.89948	0.00	1.77E-22	1.75E-22	1.1	2.76E-04
Qef 4	2682.98186	0.01	4.58E-22	4.57E-22	0.2	2.75E-04
Qef 3	2683.04751	-0.04	1.25E-22	1.24E-22	0.8	2.76E-04
Qef 2	2683.09672	0.01	2.77E-22	2.76E-22	0.4	2.76E-04
Qef 1	2683.12947	0.03	5.72E-23	5.67E-23	0.9	2.79E-04
Ree 2	2690.16193	-0.06	3.72E-23	3.66E-23	1.6	2.78E-04
Ree 3	2692.48862	0.09	1.59E-22	1.58E-22	0.6	2.73E-04
Ree 7	2701.72884	-0.06	2.83E-22	2.84E-22	-0.4	2.66E-04
Ree 8	2704.02127	-0.02	9.80E-23	9.83E-23	-0.3	2.65E-04
Ree 9	2706.30597	-0.01	2.98E-22	2.98E-22	0.0	2.64E-04
Ree10	2708.58269	0.09	9.82E-23	9.82E-23	0.0	2.63E-04
Ree11	2710.85072	-0.04	2.84E-22	2.85E-22	-0.4	2.62E-04
Ree12	2713.10999	-0.05	9.01E-23	9.00E-23	0.1	2.62E-04
Ree13	2715.35998	-0.01	2.51E-22	2.51E-22	0.0	2.60E-04
Ree14	2717.60019	0.05	7.64E-23	7.66E-23	-0.3	2.58E-04
Ree15	2719.83007	0.04	2.06E-22	2.07E-22	-0.5	2.57E-04
Ree16	2722.04921	0.03	6.09E-23	6.10E-23	-0.2	2.56E-04
Ree17	2724.25705	-0.02	1.59E-22	1.60E-22	-0.6	2.55E-04
Ree18	2726.45317	-0.04	4.57E-23	4.57E-23	0.0	2.54E-04
Ree19	2728.63714	0.00	1.16E-22	1.16E-22	0.0	2.53E-04
Ree20	2730.80834	-0.03	3.23E-23	3.23E-23	0.0	2.52E-04
Ree21	2732.96638	-0.05	7.94E-23	7.98E-23	-0.5	2.50E-04
Ree22	2735.11106	0.13	2.11E-23	2.16E-23	-2.4	2.44E-04
Ree23	2737.24135	-0.05	5.17E-23	5.19E-23	-0.4	2.48E-04

[a] See footnote of Table 3 for the meaning of column headings.

Table 7. Line parameters obtained for the $\nu_2 + (\nu_4 + \nu_5)_0^+ - \nu_4^1$ band of $^{12}C_2H_2$ [a]

Line	Position	Dif	S_{obs}	S_{calc}	%	$\lvert R \rvert^2_{obs}$
Pee23	2614.62567	-0.10	4.80E-23	4.80E-23	0.0	2.31E-04
Pee21	2619.60360	0.00	7.02E-23	7.10E-23	-1.1	2.20E-04
Pee19	2624.54935	0.03	9.88E-23	9.96E-23	-0.8	2.13E-04
Pee18	2627.01055	-0.09	3.75E-23	3.85E-23	-2.7	2.05E-04
Pee17	2629.46464	0.13	1.33E-22	1.32E-22	0.8	2.08E-04
Pee16	2631.91109	-0.05	5.13E-23	4.98E-23	2.9	2.10E-04
Pee15	2634.35067	-0.06	1.74E-22	1.66E-22	4.6	2.10E-04
Pee14	2636.78352	0.03	5.97E-23	6.07E-23	-1.7	1.94E-04
Pee11	2644.04251	0.04	2.18E-22	2.18E-22	0.0	1.89E-04
Pee10	2646.44960	0.01	7.38E-23	7.44E-23	-0.8	1.84E-04
Pee 9	2648.85070	-0.01	2.24E-22	2.24E-22	0.0	1.83E-04
Pee 7	2653.63535	0.00	2.12E-22	2.12E-22	0.0	1.78E-04
Pee 6	2656.01909	-0.02	6.60E-23	6.62E-23	-0.3	1.75E-04
Pee 5	2658.39732	0.06	1.84E-22	1.80E-22	2.2	1.77E-04
Pee 4	2660.76980	-0.06	5.18E-23	5.24E-23	-1.2	1.69E-04
Pee 3	2663.13679	-0.16	1.37E-22	1.30E-22	5.1	1.78E-04
Qef19	2667.05865	0.00	5.94E-23	5.78E-23	2.7	1.96E-04
Qef18	2667.38231	0.00	1.98E-22	2.02E-22	-2.0	1.84E-04
Qef17	2667.68703	0.01	7.62E-23	7.71E-23	-1.2	1.83E-04
Qef 7	2669.75492	0.00	1.25E-22	1.25E-22	0.0	1.67E-04
Qef 6	2669.86801	0.00	3.50E-22	3.51E-22	-0.3	1.66E-04
Qef 5	2669.96463	-0.03	1.05E-22	1.06E-22	-1.0	1.65E-04
Qef 3	2670.10923	0.03	7.36E-23	7.39E-23	-0.4	1.63E-04
Qef 2	2670.15727	0.00	1.61E-22	1.64E-22	-1.9	1.61E-04
Qef 1	2670.18928	-0.01	3.21E-23	3.34E-23	-4.0	1.57E-04
Ree 1	2674.89011	0.18	3.25E-23	3.28E-23	-0.9	1.59E-04
Ree 2	2677.22371	-0.04	2.05E-23	2.12E-23	-3.4	1.54E-04
Ree 3	2679.55185	0.06	9.16E-23	9.13E-23	0.3	1.58E-04
Ree 4	2681.87378	-0.15	3.88E-23	3.85E-23	0.8	1.57E-04
Ree 5	2684.19006	0.02	1.36E-22	1.35E-22	0.7	1.55E-04
Ree 6	2686.50006	0.09	5.00E-23	5.02E-23	-0.4	1.53E-04
Ree 9	2693.39075	0.02	1.70E-22	1.69E-22	0.6	1.51E-04
Ree10	2695.67395	-0.02	5.57E-23	5.55E-23	0.4	1.50E-04
Ree13	2702.47937	-0.01	1.43E-22	1.42E-22	0.7	1.49E-04
Ree14	2704.73225	0.02	4.35E-23	4.33E-23	0.5	1.48E-04
Ree15	2706.97681	0.01	1.17E-22	1.17E-22	0.0	1.46E-04
Ree16	2709.21278	-0.06	3.45E-23	3.46E-23	-0.3	1.46E-04
Ree17	2711.44001	-0.04	9.08E-23	9.06E-23	0.2	1.46E-04
Ree18	2713.65816	0.00	2.60E-23	2.60E-23	0.0	1.45E-04

[a] See footnote of Table 3 for the meaning of column headings.

Table 8. Summary of $^{12}C_2H_2$ vibrational transition dipole moments squared, and Herman-Wallis coefficients, obtained for the 5 bands analyzed in this work (see Eqs. (1-9))

Center[a]	Band	Vibrational symmetry	# of studied transitions	$\|R_0\|^2$ (in 10^{-5} D^2)[b]	A_1^{RP} (in 10^{-3})	A_2^{RP} (in 10^{-4})	A_2^{Q} (in 10^{-4})
2703.08	$\nu_2 + \nu_5^1$	$\Pi_u \leftarrow \Sigma_g^+$	61	2.2861(90)	5.55(18)	0	0
2681.97	$\nu_3 - \nu_4^1$	$\Sigma_u^+ \leftarrow \Pi_g$	57	27.615(70)	−2.116(97)	0	−1.613(71)
2670.21	$\nu_2 + (\nu_4 + \nu_5)_+^0 - \nu_4^1$	$\Sigma_u^+ \leftarrow \Pi_g$	39	16.34(15)	−5.33(30)	1.25(24)	2.10(36)
2642.52	$\nu_1 - \nu_5^1$	$\Sigma_g^+ \leftarrow \Pi_u$	55	51.91(12)	−3.878(93)	0	0
2560.60	$(3\nu_4 + \nu_5)_+^0$	$\Sigma_u^+ \leftarrow \Sigma_g^+$	33	0.1733(20)	0	−3.18(30)	

[a] Rough values of band centers (in cm^{-1}) are reported only as a guide.
[b] 1 debye = 3.33546×10^{-30} C·m.

Table 9. Extract of the line list of $^{12}C_2H_2$ around 3.8 μm

ν_0	S_0	R^2	γ_{air}	γ_{self}	E_{inf}	n_{air}	δ_{air}	$v_1'v_2'v_3'v_4'v_5'$ ℓ'sym'	$v_1''v_2''v_3''v_4''v_5''\ell$ "sym"	attribution	error codes
2674.890105	3.203E-23	1.601E-04	0.1043	0.1910	614.0444	0.75	-0.001	0 1 0 1 1 0+ u	0 0 0 1 0 1 g	R 1e	466643
2675.154908	6.018E-24	2.213E-04	0.0524	0.0977	1637.5056	0.75	-0.001	0 0 1 0 0 0+ u	0 0 0 1 0 1 g	Q 29f	346643
2675.222329	8.128E-23	4.643E-04	0.0768	0.1407	943.2125	0.75	-0.001	1 0 0 0 0 0+ g	0 0 0 0 1 1 u	R 13e	466643
2675.323229	3.750E-22	2.015E-05	0.0796	0.1505	155.2890	0.75	-0.001	0 1 0 0 1 1 u	0 0 0 0 0 0+ g	P 11e	466643
2675.728019	2.431E-23	2.213E-04	0.0541	0.1009	1569.1971	0.75	-0.001	0 0 1 0 0 0+ u	0 0 0 1 0 1 g	Q 28f	346643
2676.076360	2.115E-22	2.797E-04	0.0985	0.1854	625.7974	0.75	-0.001	0 0 1 0 0 0+ u	0 0 0 1 0 1 g	P 3e	466643
2676.278700	1.078E-23	2.213E-04	0.0560	0.1040	1503.2334	0.75	-0.001	0 0 1 0 0 0+ u	0 0 0 1 0 1 g	Q 27f	346643
2676.806481	4.246E-23	2.213E-04	0.0578	0.1070	1439.6155	0.75	-0.001	0 0 1 0 0 0+ u	0 0 0 1 0 1 g	Q 26f	346643
2677.223711	2.069E-23	1.586E-04	0.0985	0.1854	618.7456	0.75	-0.001	0 1 0 1 1 0+ u	0 0 0 1 0 1 g	R 2e	466643
2677.311061	1.835E-23	2.213E-04	0.0597	0.1099	1378.3447	0.75	-0.001	0 0 1 0 0 0+ u	0 0 0 1 0 1 g	Q 25f	466643
2677.372205	2.221E-22	4.605E-04	0.0756	0.1376	976.1350	0.75	-0.001	1 0 0 0 0 0+ g	0 0 0 0 1 1 u	R 14e	466643
2677.792219	7.171E-23	2.253E-04	0.0616	0.1128	1319.4218	0.75	-0.001	0 0 1 0 0 0+ u	0 0 0 1 0 1 g	Q 24f	466643
2677.803193	1.292E-22	2.039E-05	0.0808	0.1541	129.4115	0.75	-0.001	0 1 0 0 1 1 u	0 0 0 0 0 0+ g	P 10e	466643
2678.250295	3.071E-23	2.292E-04	0.0635	0.1155	1262.8480	0.75	-0.001	0 0 1 0 0 0+ u	0 0 0 1 0 1 g	Q 23f	466643
2678.438683	5.454E-23	2.785E-04	0.1043	0.1910	618.7456	0.75	-0.001	0 0 1 0 0 0+ u	0 0 0 1 0 1 g	P 2e	466643
2678.685280	1.167E-22	2.329E-04	0.0653	0.1183	1208.6241	0.75	-0.001	0 0 1 0 0 0+ u	0 0 0 1 0 1 g	Q 22f	466643
2679.097259	4.858E-23	2.365E-04	0.0671	0.1210	1156.7513	0.75	-0.001	0 0 1 0 0 0+ u	0 0 0 1 0 1 g	Q 21f	466643
2679.486637	1.794E-22	2.400E-04	0.0688	0.1237	1107.2302	0.75	-0.001	0 0 1 0 0 0+ u	0 0 0 1 0 1 g	Q 20f	466643
2679.508175	6.633E-23	4.567E-04	0.0746	0.1347	1011.4062	0.75	-0.001	1 0 0 0 0 0+ g	0 0 0 0 1 1 u	R 15e	466643
2679.551851	8.925E-23	1.571E-04	0.0940	0.1801	625.7974	0.75	-0.001	0 1 0 1 1 0+ u	0 0 0 1 0 1 g	R 3e	466643
2679.853904	7.255E-23	2.433E-04	0.0704	0.1264	1060.0618	0.75	-0.001	0 0 1 0 0 0+ u	0 0 0 1 0 1 g	Q 19f	466643
2680.199399	2.601E-22	2.465E-04	0.0719	0.1291	1015.2468	0.75	-0.001	0 0 1 0 0 0+ u	0 0 0 1 0 1 g	Q 18f	466643

Note: ν_0 is the wavenumber of the transition in cm^{-1}, S_0 is the calculated line intensity for natural abundances of C_2H_2 at 296 K in cm.molecule^{-1}, R^2 is the calculated transition dipole moment squared for pure $^{12}C_2H_2$ in debye^2, γ_{air} and γ_{self} are respectively the air- and self-broadening coefficients in cm^{-1}.atm^{-1} at 296 K, E_{inf} is the energy of the lower level in cm^{-1}, n_{air} is the temperature dependence of the air-broadening coefficient at 296 K, δ_{air} is the air-shifting coefficient in cm^{-1}.atm^{-1}, $v_1'v_2'v_3'v_4'v_5'$ ℓ' sym' and $v_1''v_2''v_3''v_4''v_5''$ ℓ " sym" are, respectively for the upper and lower state, the quantum numbers in the vibrational modes v_1, v_2, v_3, v_4, and v_5, the secondary vibrational quantum number, and the symmetry of the vibrational state [13], attribution corresponds to the rotational assignment of the transition (the type of branch, the rotational quantum number J, and the rovibrational symmetry e or f), and finally the error codes related to the wavenumber, the intensity, the air- and self-broadening coefficients, the temperature dependence, and the air-shifting coefficient (see text for details).

Fig. 1. Overview of the 5 spectra recorded in this work with the Bruker IFS 120 interferometer of the LADIR. We assigned a number from 1 to 5 to these experimental spectra (see Table 1 for details). Four spectral regions of noticeable absorption are observed: around 2200 cm^{-1} where one can see the $3\nu_5^1$ band of $^{12}C_2H_2$ used to check the purity of the gas (see text); around 2350 cm^{-1} where the absorption of the strong ν_3 band of $^{12}C^{16}O_2$ (used for the wavenumber calibration, see text) is due to small traces of this gas in the sample; around 2700 cm^{-1} where one can see the 5 strongest bands of $^{12}C_2H_2$ studied in this work; and finally the strong absorption of numerous bands of $^{12}C_2H_2$ around 3300 cm^{-1}.

Fig. 2. This figure represents the whole Q_{fe} branch of the $\nu_2 + \nu_5^1$ band observed in 4 experimental spectra recorded in this work (numbers 1-4, see Table 1), and the difference (noted obs–calc) between these experimental spectra and those which are simultaneously adjusted with the multispectrum fitting procedure. The spectral domain adjusted during the fit is equal to 1.4 cm^{-1}, so that all the lines of the whole Q branch were fitted simultaneously in the 4 spectra together.
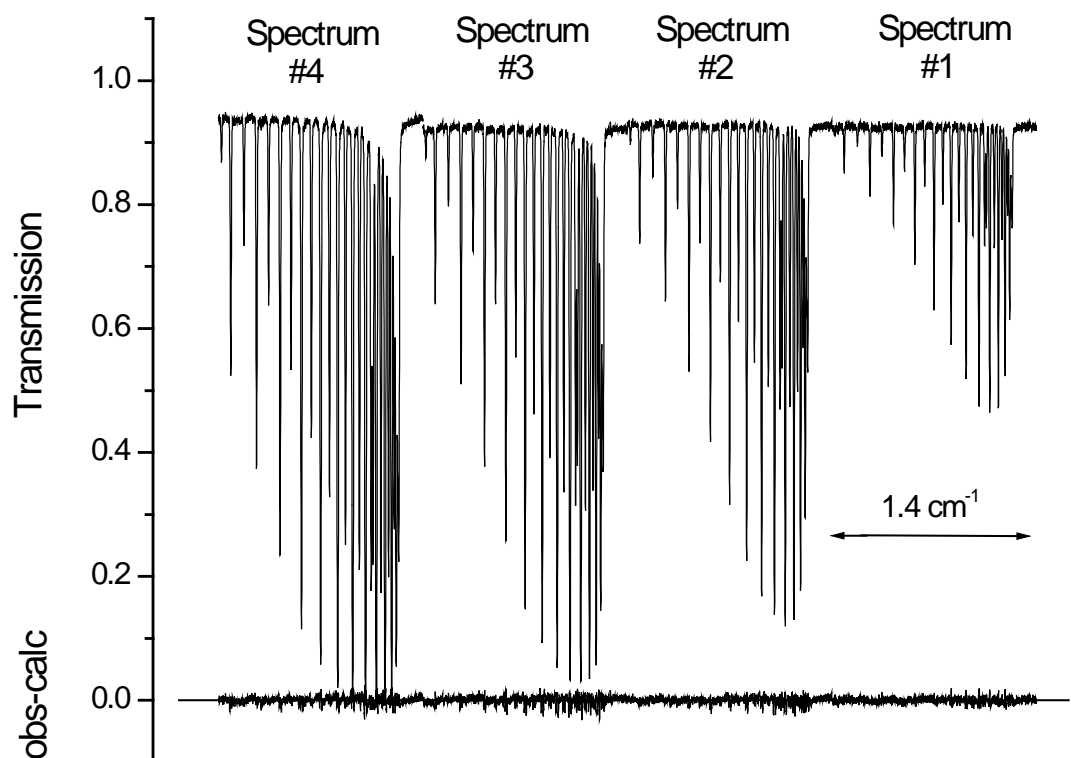
Fig. 3. Wavenumber calibration factor $\varepsilon = (\nu_{HITRAN2004} - \nu_{this\ work})/\nu_{HITRAN2004}$ obtained for transitions of the ν_3 band of $^{12}C^{16}O_2$ in the 5 experimental spectra of this work. The straight line represents the average value $\langle\varepsilon\rangle = 1.285(32)\times10^{-6}$ which means a shift of $3.33(6)\times10^{-3}$ cm^{-1} at 2600 cm^{-1} (numbers of the spectra refer to those of Table 1).
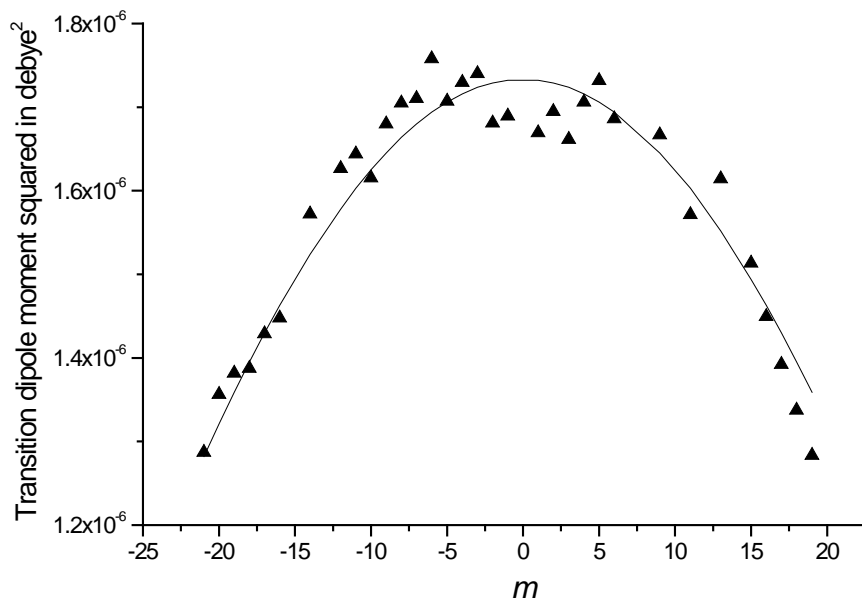
Fig.4. Experimental and calculated values of the transition dipole moment squared of the $\nu_2 + \nu_5^1$ band. Black triangles are for P_{ee} and R_{ee} lines, and black squares for Q_{fe} lines. The curves have been calculated using the constants found in this work (see Table 8).

Fig.5. Experimental and calculated values of the transition dipole moment squared of the $(3\nu_4 + \nu_5)_0^+$ band. Black triangles are for P_{ee} and R_{ee} lines. The curves have been calculated using the constants found in this work (see Table 8).

Fig.6. Experimental and calculated values of the transition dipole moment squared of the $v_1 - v_5^1$ band. Black triangles are for P_{ee} and R_{ee} lines, and black squares for Q_{ef} lines. The curves have been calculated using the constants found in this work (see Table 8).
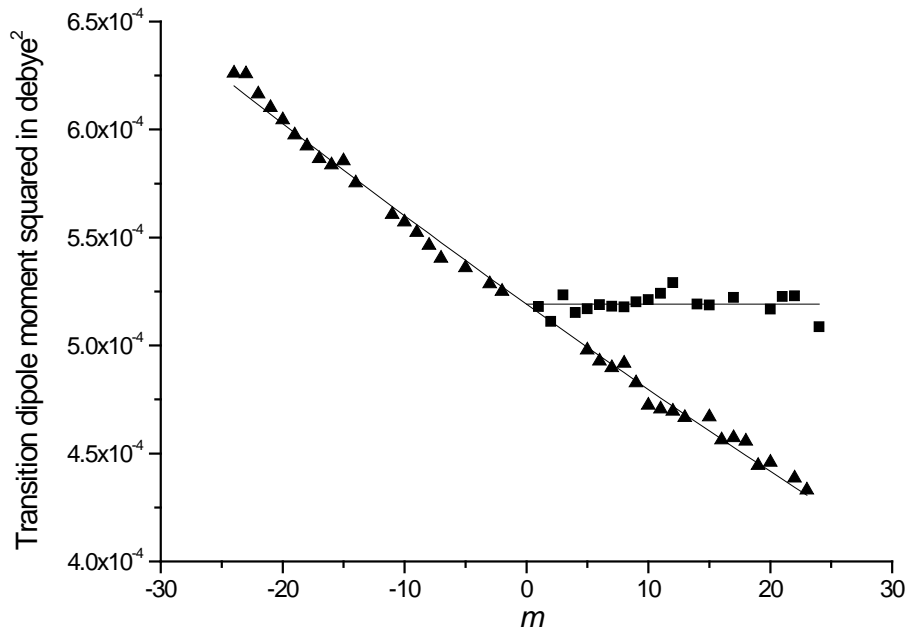
Fig.7. Experimental and calculated values of the transition dipole moment squared of the $\nu_3 - \nu_4^1$ band. Black triangles are for P_{ee} and R_{ee} lines, and black squares for Q_{ef} lines. The curves have been calculated using the constants found in this work (see Table 8).
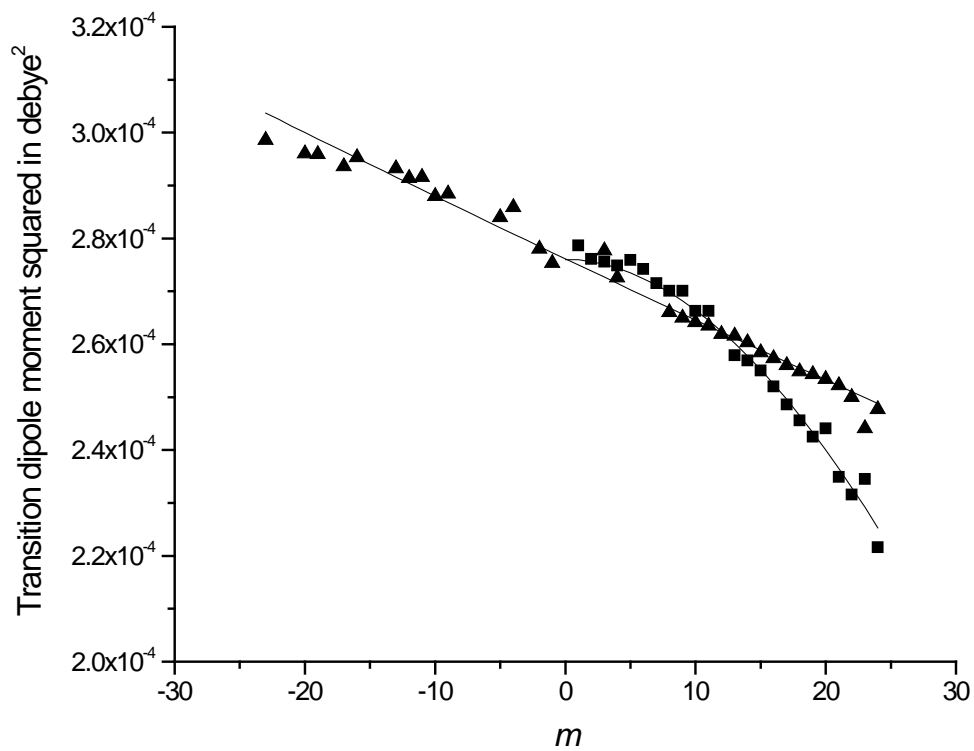
Fig.8. Experimental and calculated values of the transition dipole moment squared of the $\nu_2 + (\nu_4 + \nu_5)_0^+ - \nu_4^1$ band. Black triangles are for P_{ee} and R_{ee} lines, and black squares for Q_{ef} lines. The curves have been calculated using the constants found in this work (see Table 8).